Midlatitude Jet Position Spread Linked to Atmospheric Convective Types

Fuchs, David; Sherwood, Steven C.; Waugh, Darryn; Dixit, Vishal; England, Matthew H.; Hwong, Yi-Ling; Geoffroy, Olivier

DOI
10.1175/JCLI-D-21-0992.1

Publication date
2023

Document Version
Final published version

Published in
Journal of Climate

Midlatitude Jet Position Spread Linked to Atmospheric Convective Types

DAVID FUCHS,[a] STEVEN C. SHERWOOD,[a,b] DARRYN WAUGH,[c] VISHAL DIXIT,[d] MATTHEW H. ENGLAND,[a,b] YI-LING HWONG,[a,b] AND OLIVIER GEOFFROY[e]

[a] *Climate Change Research Centre, University of New South Wales, Sydney, New South Wales, Australia*
[b] *ARC Centre of Excellence for Climate Extremes, University of New South Wales, Sydney, New South Wales, Australia*
[c] *Department of Earth and Planetary Sciences, Johns Hopkins University, Baltimore, Maryland*
[d] *Department of Remote Sensing and Geosciences, Delft University of Technology, Delft, Netherlands*
[e] *Centre National de Recherches Météorologiques, Météo-France, CNRS, Toulouse, France*

(Manuscript received 23 December 2021, in final form 31 August 2022)

ABSTRACT: Midlatitude weather is largely governed by bands of strong westerly winds known as the midlatitude jets, but what controls the jet properties, particularly their latitudes, remains poorly understood. Climate models show a spread of about 10° in their simulated present-day latitude of the Southern Hemisphere (SH) jet, and a related spread in its predicted poleward shift under global warming. We find that models with more poleward jets simulate more low-level moisture, a warmer upper troposphere, and different precipitation patterns than those with equatorward jets, potentially implicating intermodel differences in moist convection and microphysics. Accordingly, a suite of atmospheric model runs is performed where the deep or shallow convective parameterizations are individually turned off either globally or in specific latitude bands. These experiments suggest that models that produce more shallow convection in the midlatitudes tend to position the jet relatively poleward in SH summer, whereas those that favor deep convection tend to position it equatorward. This accounts for a spread 60% as large as that of the AMIP ensemble during the austral summer. Our results suggest that, in the boreal summer, similar biases appear in the Northern Hemisphere. The presence of shallow convection in the Northern Hemisphere midlatitudes reduces SH jet shift in a warmer climate in accordance to the correlation between jet positions and shift seen in this season. These results can help explain intermodel differences in the position and shift of the jet, and point to an unexpected role for atmospheric moist convection in the midlatitude circulation.

KEYWORDS: Atmospheric circulation; Convection; Jets; Climate change; Convective-scale processes; Convective parameterization

1. Introduction

Arguably the most prominent feature of the general circulation of Earth's atmosphere is the midlatitude jets. These relate to the location of midlatitude storms, and influence weather in midlatitudes (Wallace and Hobbs 2006). The location of the jets influences the global atmospheric circulation, through, for example, connections with the Hadley cell (Kang and Polvani 2011; Butler et al. 2011). The upper-tropospheric jets exert a significant stress at the surface. The surface wind stress due to the SH surface westerlies influences the ocean circulation and uptake of heat and carbon (Fyfe and Saenko 2006; Le Quéré et al. 2007; Waugh et al. 2013; Armour et al. 2016). Thus, the latitude of the jet affects midlatitude weather and global climate.

Observations indicate a poleward shift in the SH jet in recent decades (Davis and Rosenlof 2012; Swart and Fyfe 2012), primarily as a result of seasonal polar stratospheric ozone depletion (Barnes et al. 2014). Climate models agree that the jets move poleward in response to greenhouse gas (GHG) increases, and project further poleward displacement at the end of this century (Barnes and Polvani 2013; Grise and Polvani 2014; Vallis et al. 2015), as the climate response to rising GHG concentration outweighs stratospheric ozone recovery. However, there is a substantial spread in mean latitude of the SH jet in models that participated in the most recent Coupled Model Intercomparison Projects (CMIP5 and CMIP6), with many models locating this jet equatorward of its observed position (Fyfe and Saenko 2006; Swart and Fyfe 2012). This not only affects simulated storms, precipitation, and ocean circulation, but also likely biases the projected latitudinal shifts in the jets, which at least in the SH are generally larger in models with a more equatorward bias in present-day simulations (Vallis et al. 2015; Kidston and Gerber 2010; Son et al. 2010; Bracegirdle et al. 2013; Simpson et al. 2021).

The reason for the spread in predicted jet latitudes, and the link to future changes, remains a mystery. Factors known to contribute to jet bias are model resolution and surface drag (Pithan et al. 2016; Lindvall et al. 2017), sea surface temperature gradients (Michel and Rivière 2014; Brayshaw et al. 2008), and cloud radiative heating (Voigt and Shaw 2015; Li et al. 2015; Watt-Meyer and Frierson 2017). It has been suggested that jet biases arise due to biases in the cloud reflectance of sunlight, via its influence on the meridional gradient of sea surface temperatures (SSTs), hence the regions of baroclinicity and the jet latitude (Ceppi et al. 2014). While this may contribute to the jet bias it cannot be the dominant

Supplemental information related to this paper is available at the Journals Online website: https://doi.org/10.1175/JCLI-D-21-0992.s1.

Corresponding author: David Fuchs, d.fuchs@unsw.edu.au

DOI: 10.1175/JCLI-D-21-0992.1

mechanism, as a comparable spread and bias occur in model runs with SSTs fixed to observed values (Bracegirdle et al. 2013). Thus, the main cause for the bias cannot be linked to SSTs. Notably, the jet position was reported to be sensitive to cloud parameters in at least one model (Hourdin et al. 2013).

Here we show that a key reason leading to intermodel differences in SH jet position is that the position is sensitive to an aspect of moist convection that is not well understood or consistently treated in global atmospheric models. Moreover, the same sensitivity appears to drive much of the diversity in projected future climate responses of the SH jet, with implications for important aspects of weather and climate.

2. Data and methods

The analysis in this study is based on monthly mean model outputs from CMIP5 and CMIP6 (Taylor et al. 2012; Eyring et al. 2016), as well as runs performed with the Community Atmospheric Model (CAM; Neale et al. 2010). Data from ocean–atmosphere coupled runs are based on 42 models in the preindustrial control ensemble (piControl). Lapse rate and jet positions were found to be similar between historical and piControl scenarios, so only the latter were used. Experiments with fixed SST conditions use 44 atmospheric global circulation models (AGCMs) from both CMIP5 and CMIP6 Atmospheric Model Intercomparison Project (AMIP), most of which are also present in the piControl experiment. These were also repeated for models from the CMIP6 ensemble only. A subset of these models also offer data for a climate warming scenario where SST is uniformly increased by 4 K. This includes the CMIP5 AMIP-4K and CMIP6 AMIP-P4K ensembles (hereafter the term AMIP-4K will refer to both CMIP ensembles), which are part of the second and third phases of the Cloud Feedback Model Intercomparison Project (Bony et al. 2011; Webb et al. 2017). Finally, the ERA-Interim data product is used for observational reference (Dee et al. 2011).

Further investigation is done using version 4 of CAM from the Community Earth System Model release 1.0.6 (CAM4; Neale et al. 2010). CAM4 parameterizes convection using two separate schemes. Parameterization of deep convection is based on Zhang and McFarlane (1995), which is a mass-flux scheme that represents updrafts and associated downdrafts when the atmosphere is conditionally unstable in the lower troposphere. Parameterization of shallow convection is based on Hack (1994), which mixes adjacent layers when they are locally unstable. As such this scheme does not represent updrafts or downdrafts explicitly and does not represent nonlocal transport of heat and moisture the way the deep scheme does. This shallow scheme was the only convective scheme present in versions of the NCAR model prior to the development of the Zhang–McFarlane deep scheme in the mid-1990s. In CAM4 this scheme executes after the deep scheme and, as noted by Hack (1994), tends to significantly moisten and warm the troposphere compared to the moist adjustment scheme that preceded its introduction to CAM. The tendency of shallow convection to moisten the troposphere is not limited to the Hack scheme. For example, Neggers et al. (2007) coined the term *shallow cumulus humidity throttle*, abstracting the role of shallow convection as a source of moisture in the onset of deep convection. The tendency of shallow convection to moisten the troposphere will play a key part in our work.

Simulations with CAM4 used climatological mean preindustrial SST conditions (F1850 scenario), 1.9° × 2.5° resolution, and 26 hybrid vertical levels. Selected runs were performed using the AMIP scenario to ensure that differences to the F1850 scenario are small. To accurately determine the climatology and remove internal variability, CAM4 configurations were run for a 40-yr period. Several CAM4 runs were performed, where deep and shallow convection were disabled either globally or in selected latitudes (see section 4). Shallow convection was inhibited by zeroing the Hack scheme tendencies after its execution, whereas deep convection was inhibited by setting a large convective available potential energy (CAPE) limit triggering threshold so that the scheme would never activate.

The positions of the midlatitude jets were calculated as in Kidston and Gerber (2010); namely, the grid point i with maximum zonal-mean zonal wind speed at 850 hPa was found in the SH. A quadratic fit was then applied on grid values $i - 1$, i, and $i + 1$. The jet position is then defined as the maximum value of the quadratic fit in the grid segment $[i - 1; i + 1]$ after the data were interpolated to 0.01° resolution (Kidston and Gerber 2010).

Our analysis also requires us to calculate two additional metrics. First, the seasonal eddy kinetic energy (EKE) is defined as

$$\frac{1}{2}(u'^2 + v'^2), \tag{1}$$

where u' and v' are deviations from the time mean of the zonal and meridional components of wind. To be comparable with Frierson et al. (2007), in AMIP these were calculated at 600 hPa based on monthly data and then averaged to season and meridional location. In addition, seasonal zonal-mean meridional temperature differences between the tropics and the pole are defined as

$$\overline{T_{20°S–20°N}} - \overline{T_{60°–90°S}}, \tag{2}$$

where the overbar denotes area-weighted mean for the given latitudes and season, between pressure levels 200 and 925 hPa. Notably, this definition excludes the midlatitudes.

3. Exploring the spread of jet positions in CMIP/AMIP ensembles

We seek to explain the spread of climatological jet positions in model ensembles with and without SST constrained to observations. Simulations in piControl ocean–atmosphere coupled CMIP ensemble, show jet latitude spread of about 9° in DJF and 17° in JJA (Simpson et al. 2020; see also Table S2 in our online supplemental material and Figs. 5a,b). A similar spread occurs in a suite of atmosphere-only model runs from the AMIP ensemble, which includes many of the same atmosphere models used in CMIP (Table S2 and Figs. 5c,d). In both seasons, this broad spread occurs even though all the AMIP runs prescribe the same sea surface temperatures.

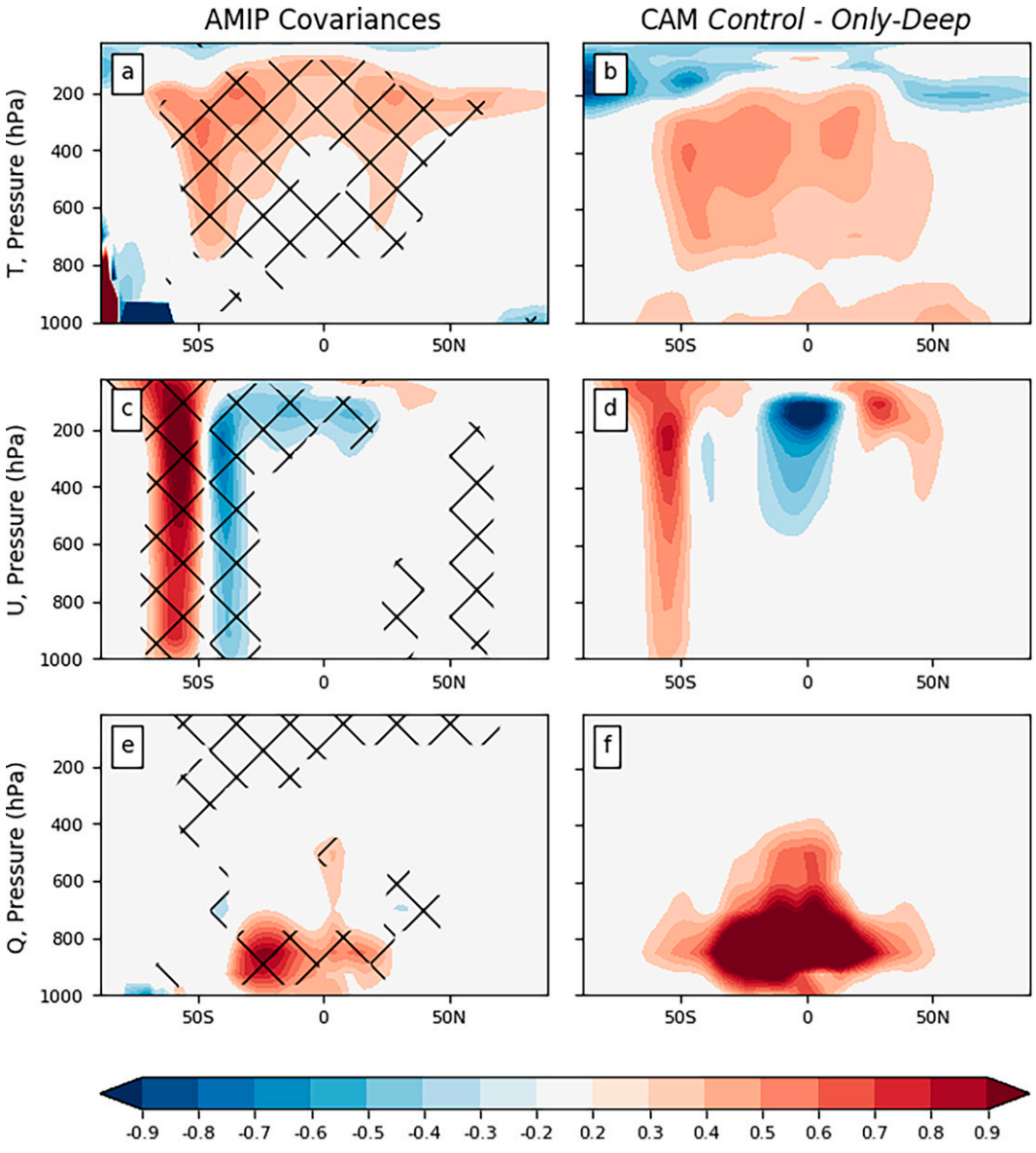

FIG. 1. Relationship between climatological SH jet position and climatological zonal and seasonal mean of selected variables during DJF. (left) Covariances in the AMIP ensemble and (right) differences of CAM4 Control configuration minus the Only-Deep configuration divided by the difference in jet positions. Further details related to CAM4 configurations are given in section 4 and Table 1. (top to bottom) Zonal-mean temperature (K × degrees south) normalized by 1/4, zonal wind speed (m s^{-1} × degrees south) normalized by 1/6, and specific humidity (g kg^{-1} × degrees south). Stippling in the left column denotes significance at the 95% confidence interval ($|r| > 0.3$ assuming an independent sample).

Thus, although a bias in ocean temperatures is typically shifting the jet in the coupled models (e.g., Wood et al. 2020), the model spread is dominated by differences in atmospheric processes (see also Bracegirdle et al. 2013), and for this reason we will focus mainly on AGCM runs here.

a. *Relationship to state variables*

A number of state variables appear to be significantly related to the jet position among the AGCMs, based on simple correlation analysis, providing clues on why the jet positions vary. Around the latitude of the jet, the covariance structure shows a distinct dipole pattern for wind speed (Figs. 1c and 2c). This is expected and to first order just shows the jet shift itself. Less obvious, but consistent with Menzel et al. (2019), the subtropical jet is also stronger for models with more equatorward jet (see also Ceppi and Hartmann 2013). Particularly in DJF, temperatures in much of the troposphere are significantly correlated to jet position (Figs. 1a and 2a). The strongest

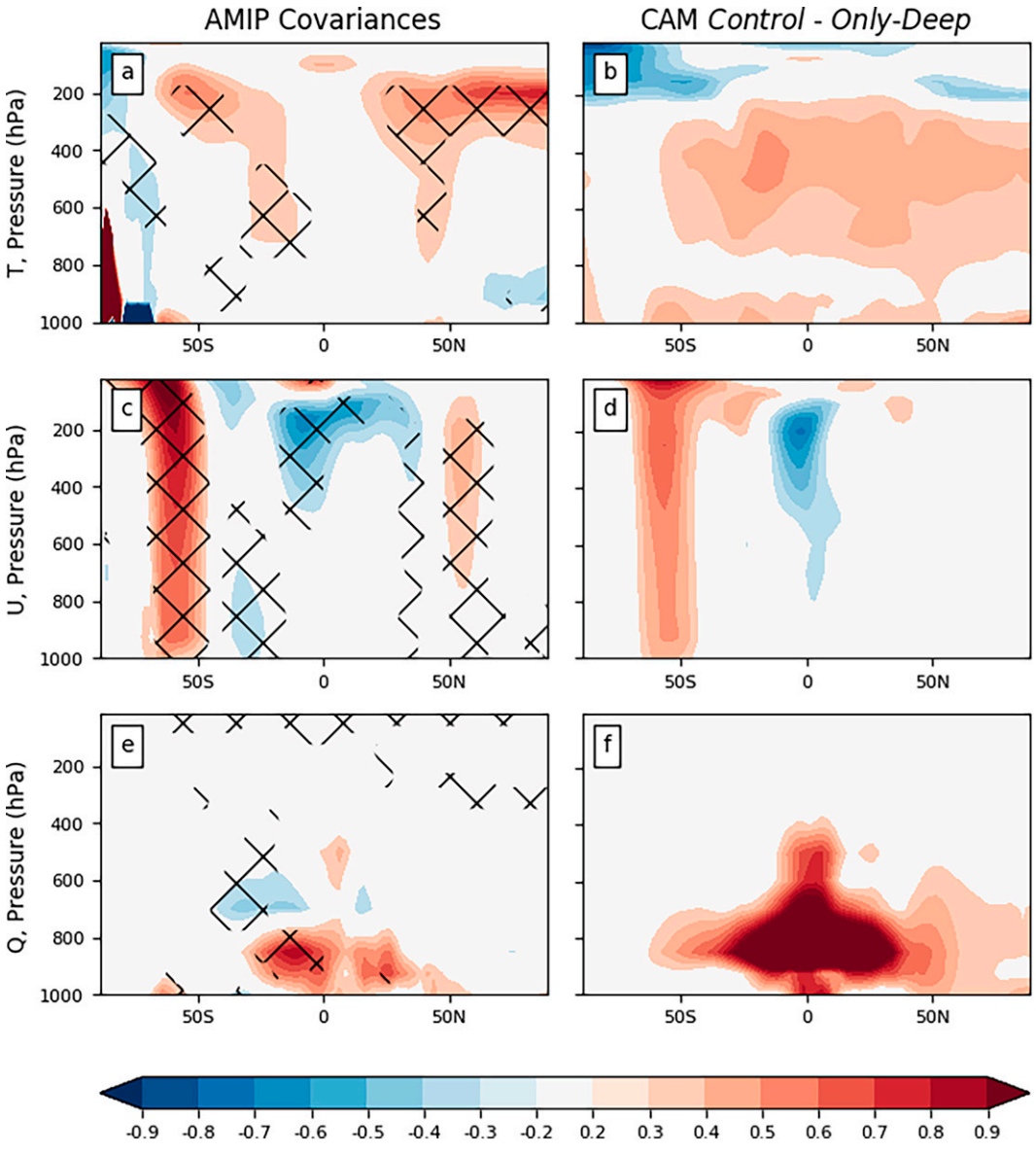

FIG. 2. As in Fig. 1, but for JJA.

relationships are near the SH jet, which could be directly related to the jet position via thermal wind balance, since the jet coincides with a strong meridional temperature gradient. However, significant correlations also exist throughout most of the upper troposphere equatorward of the jets in DJF, and throughout the Northern Hemisphere in JJA, all of which are warmer in models with poleward jets. More poleward jets also correlate with higher specific humidity in the boundary layer throughout the tropics and subtropics (Figs. 1e and 2e). These humidity changes roughly coincide with those of temperature aloft, but not always; for example, in DJF, a significant humidity signal does not appear close to the SH jet itself even though the temperature signal aloft peaks there (Fig. 1e). This suggests that the temperature changes aloft are not only due to differences in boundary layer moist static energy.

b. *Relationships to precipitation*

The jet position also shows some interesting relationships to precipitation patterns, shown for DJF in Fig. 3a and for JJA in Fig. 4a. One prominent feature is a dipole of positive values on the poleward flank of the SH storm tracks and negative on the equatorward flank, which just indicates the shift of precipitation with the jet. This appears to be more zonally consistent in DJF, while changing sign in the Atlantic Ocean in JJA. Significant covariance also appears in the tropics, where in DJF a more poleward SH jet is associated with more precipitation over the Amazon and north of the equator

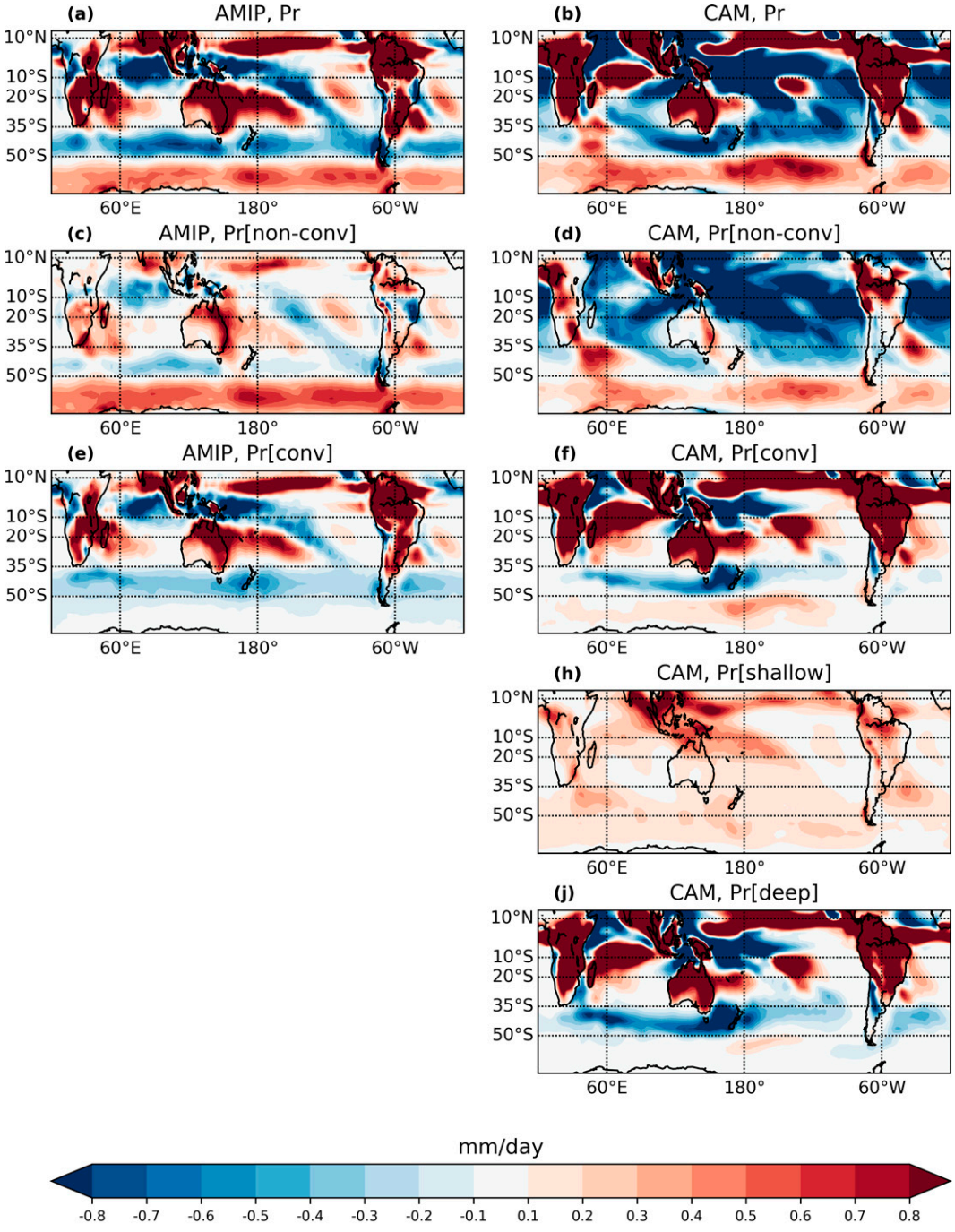

FIG. 3. Precipitation differences between models with poleward vs equatorward jet positions in DJF, showing (left) covariances with jet position in the AMIP ensemble and (right) the difference between CAM4 Control minus Only-Deep configurations, for (top to bottom) total, large-scale, convective, shallow, and deep precipitation patterns. Units in the left column are mm day^{-1} × degrees south whereas units in the right column are mm day^{-1}.

across the Indo-Pacific, suggesting a stronger Pacific intertropical convergence zone (ITCZ). In JJA, positive tropical covariance patterns shift south of the equator along the Indian Ocean and the western Pacific Ocean. Note that Figs. 3 and 4 show covariances of precipitation rather than correlations and in magnitude, the tropical precipitation signals are considerably larger than those directly associated with the shift of the SH jet. Another difference across seasons can be seen around 35°S; in DJF, equatorward from this latitude is marked by positive covariance over and to the east of continents and

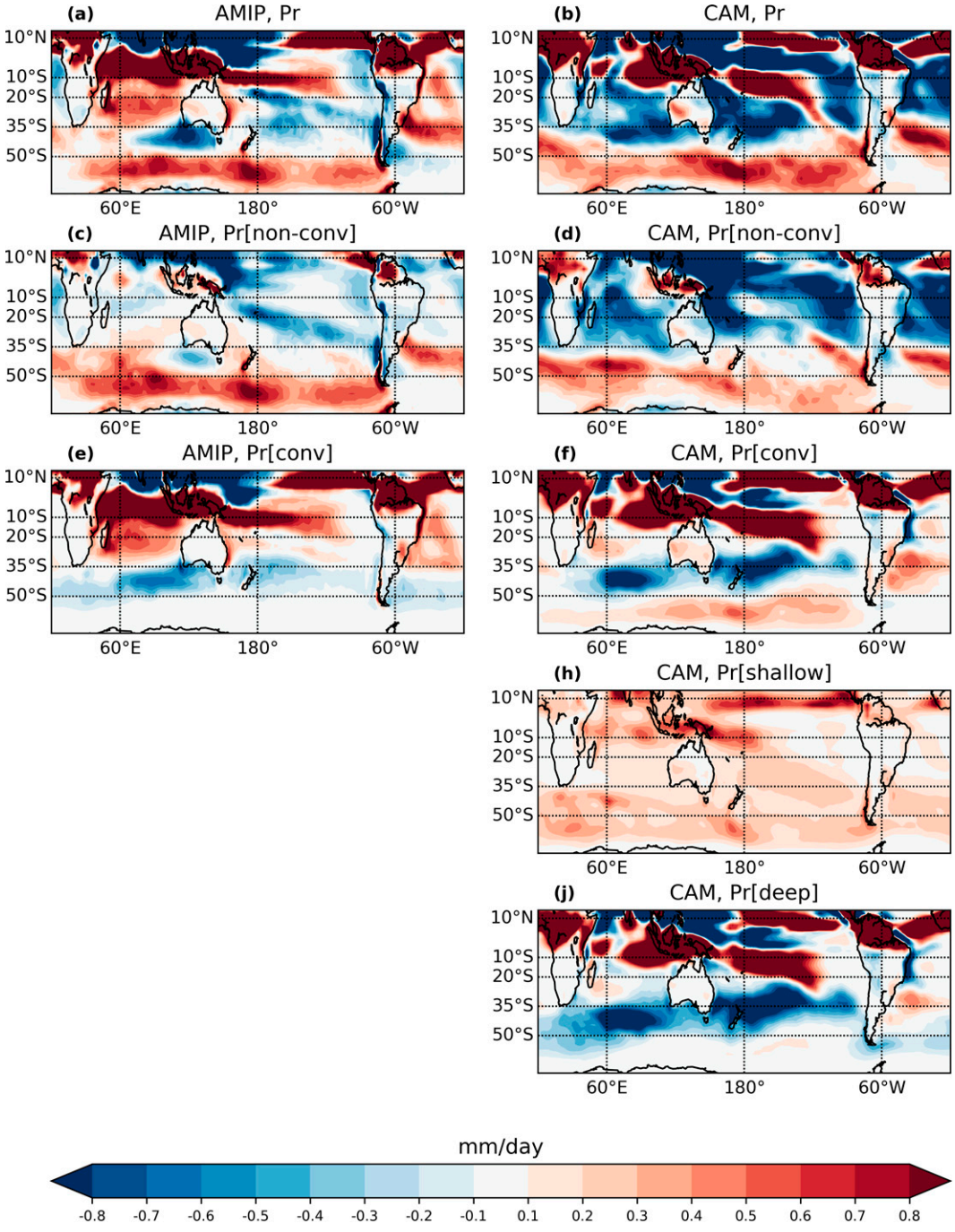

FIG. 4. As in Fig. 3, but for JJA.

negative covariances poleward from this latitude. These patterns diminish in JJA, particularly over the Pacific Ocean.

The above covariances, in particular, those between the jet position, temperature, and precipitation along the ITCZ, and midlatitude moisture, suggest that key atmospheric processes leading to spread in jet positions are convective or cloud-microphysical processes, the parameterizations of which are diverse in models (Arakawa 2004; Ceppi et al. 2016). Variables that might be expected to affect tropical temperature would be entrainment in convection (which dilutes the moist static energy of rising air, reducing its temperature), boundary layer relative humidity (which can be affected by downdrafts or shallow convection), and microphysical processes associated with latent heat of fusion (which boost the moist static energy and temperature of air upon freezing of condensed water, and the reverse when the ice melts). Indeed, the regions of strongest

temperature signal are at levels where mixed liquid and frozen cloud condensate are found near or above the freezing level (Figs. 1a and 2a). We note that although previous work suggests that cloud-radiative effects are important in determining the jet position (Li et al. 2015; Voigt and Shaw 2015), we do not find strong correlations with top-of-atmosphere radiation variables at any latitude in the AMIP runs (Fig. S1), which argues against this being a primary cause of the spread when SSTs are fixed, although cloud shading could be more important in an ocean–atmosphere coupled setting (Ceppi et al. 2014).

Following the above reasoning we break the precipitation in the AMIP ensemble into large-scale and convective components (where the convective component is that part generated directly by the convective scheme or schemes in the model). This decomposition shows that the tropical patterns are dominated by convective precipitation (Figs. 3e and 4e), although the large-scale precipitation shows similar though weaker patterns (Figs. 3c and 4c). A more interesting result emerges for the extratropical dipole pattern in the SH, where models with equatorward jet have more convective precipitation along the equatorward flank of the ensemble, while models with poleward jets tend to have more large-scale precipitation along the poleward flank. This raises the possibility that differences in the convective schemes are contributing to the jet position according to whether or not they act on the equatorward flank of the jet.

4. Convection on–off experiments

To test these ideas further we conduct experiments with the CAM, perturbing selected processes in the model. It is expected that a process that is responsible for the spread of jet positions in the AMIP ensemble would also reproduce the covariance patterns seen in Figs. 1–4. Our base hypothesis implies a link to moist convection. To test this, parameterized convection is first deactivated, following the Selected Process On/Off Klima Intercomparison Experiment (SPOOKIE; Webb et al. 2015), in which this was done with eight atmosphere-only models. In CAM4 this is achieved by turning both deep and shallow convective parameterization off. Shallow convection in CAM4 tends to redistribute moisture across a few model levels without precipitating (Hack 1994), while deep convection tends to precipitate, thus drying the column. The deep scheme also produces penetrative downdrafts that can create cold and dry anomalies near the surface, whereas the shallow scheme is expected to mix the boundary layer and hence damp anomalies. Noting the positive relation between lower-tropospheric moistening in the lower midlatitudes and the position of the jet (Figs. 1e and 2e), additional CAM4 configurations are added where deep and shallow convective parameterizations are turned off one at a time. There is clearly a potential for these two schemes to interact, so it is important to consider all combinations of the two schemes being on or off without expecting a priori that the impacts will necessarily be linear. While running each scheme separately is not entirely equivalent to having no shallow or deep convection, we explore whether this approach might capture the spread of convective behavior and/or jet behavior seen in the AMIP ensemble. The resulting CAM4 configurations will be denoted as Conv-Off, Only-Shallow, Only-Deep, and Control (see also Table 1). The Control configuration produces similar results to the slightly older version of CAM that was used in AMIP (Figs. 5c,d, dark blue marker).

TABLE 1. CAM4 base configurations.

Alias	Description
Control	Prescribed preindustrial ice and ocean climatology (F1850)
Conv-Off	Deep and shallow convection turned off
Only-Deep	Shallow convection turned off
Only-Shallow	Deep convection turned off

The jet positions from these four CAM4 configurations, and several others to be discussed shortly, are shown in Figs. 5e and 5f. The Conv-Off, Only-Shallow, and Only-Deep configurations are shown respectively as white, green, and red diamonds, and compared with the Control configuration (blue diamond). These shows that, in DJF, the CAM4 ensemble is bounded by the Only-Shallow and Only-Deep configurations, rather than when the convection is turned off entirely. In both seasons, the Only-Shallow configuration positions the jet poleward from the Control, while the Only-Deep configuration positions it equatorward from the Control. However, whereas in JJA the Only-Shallow and Only-Deep configurations span about a third of the range of the AMIP ensemble, in DJF they span most (though not all) of the AMIP ensemble, indicating that convective effects are secondary in winter but primary in summer.

We refer to the covariances of the jet with state variables in AMIP (left columns in Figs. 1 and 2) and compare them to the difference between the Control and Only-Deep configuration, highlighting the contribution of shallow convection in CAM4. Including shallow convection in CAM4 leads to a warmer midlatitude troposphere in DJF and JJA and warmer tropical troposphere in DJF (Figs. 1b and 2b). This temperature signal is in the same general direction as that of the AMIP ensemble, but with a somewhat different latitude–height pattern. The wind (Figs. 1d and 2d) and moisture (Figs. 1f and 2f) signals in CAM4 qualitatively resemble those of AMIP, albeit with a stronger moisture signal and a weaker wind signal. Interestingly, the overall stronger eddy-driven jet seen in poleward-jet AMIP models are reproduced by CAM4 with the addition of shallow convective parameterization. Thus, for key state variables, there is overall a fairly good agreement between CAM4 shallow convection on–off experiments and the AMIP ensemble, which coincides with a more poleward jet position when shallow convective parameterization is enabled in CAM4.

This agreement is even more remarkable when examining precipitation. In DJF, features that were associated with poleward jets in the AMIP ensemble are reproduced in the shallow convection on–off experiments in CAM4 (Figs. 3 and 4)—in particular, the rainfall maxima on and to the east of the continents, the maximum in the ITCZ regions north of the equator, and the minima through much of the equatorial region around

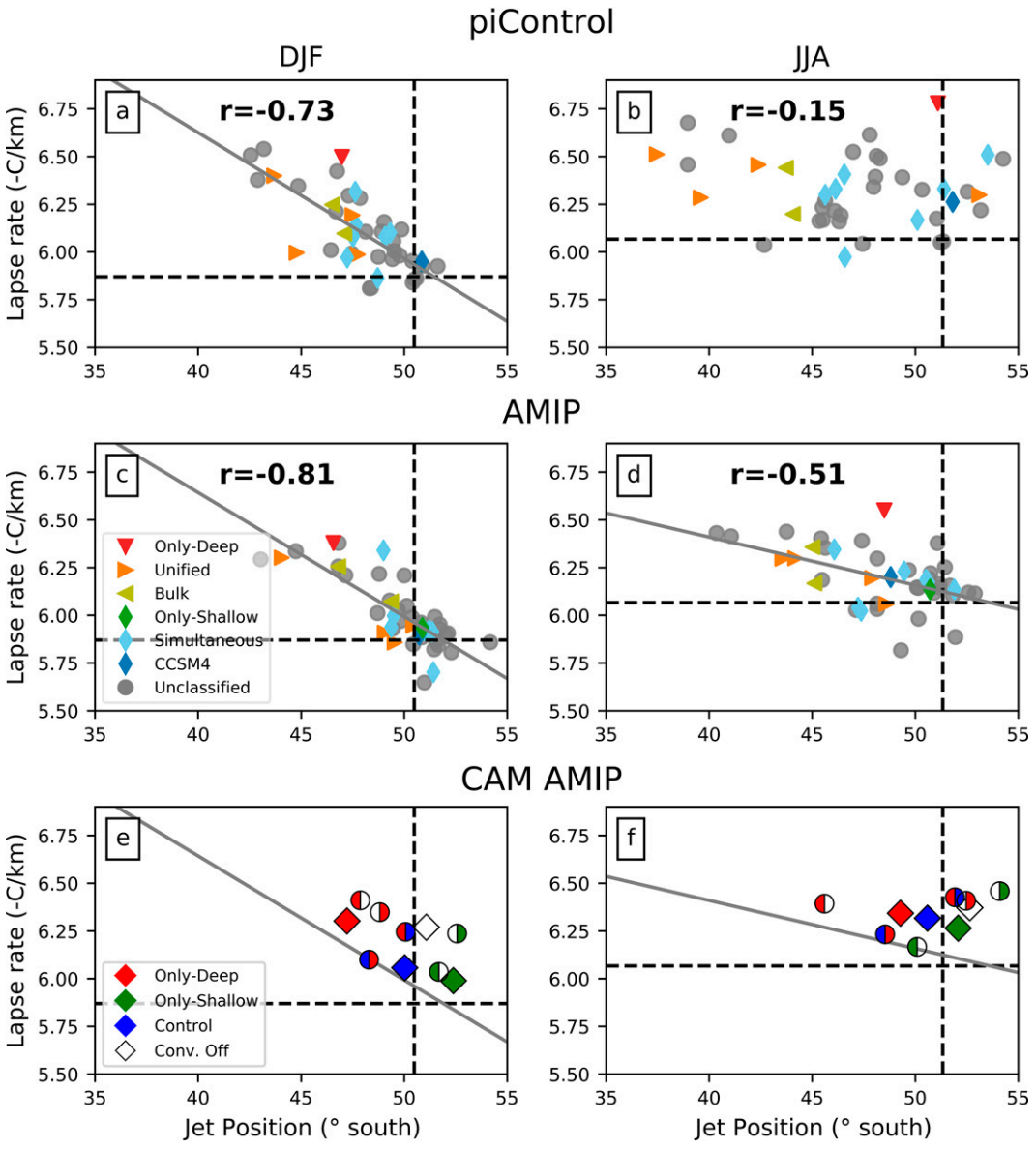

FIG. 5. Relationship between midlatitude lapse rate and SH jet position in (left) DJF and (right) JJA, showing (a),(b) CMIP5 and CMIP6 piControl, (c),(d) AMIP, and (e),(f) CAM F1850. Lapse rate is integrated between 925 and 300 hPa and 50°–20°S (refer to section 5 for details). Dashed lines mark climatological values from ERA-Interim. The line of best fit in (c) and (d) is repeated in (e) and (f) respectively. Markers in (a)–(d) follow the classification in Table 2, with Group A denoted by diamonds, Group B by triangles, and unclassified models by gray circles (further details in section 6). In (e) and (f), red, green, blue, and empty shapes indicate the Only-Deep, Only-Shallow, Control, and Conv-Off configurations (Table 1). Diamond shapes denote base configurations, while left (right) color marks the configuration that is applied inside (outside) latitudes 20°S–20°N.

Indonesia (Figs. 3b and 4b). The AMIP breakdown between convective and large-scale precipitation roles is also approximately reproduced in the jet region, with a convective signal on the equatorward flank and a large-scale signal on the poleward, although CAM4 produces a large decrease in large-scale precipitation throughout most of the tropics and subtropics that is absent in the AMIP ensemble (Figs. 3d,f and 4d,f).

Since the convection on–off experiments have revealed a mechanism for altering the jet position, we performed a series of additional experiments, with convection altered only in restricted latitude bands (shown as additional symbols in Fig. 5). The idea here is to clarify where convective physics is actually affecting the jet. First, we consider the DJF season. Adding shallow convection in the tropics only, on top of the Only-Deep configuration, results in only a small

poleward jet shift compared to the Only-Deep configuration (Fig. 5e, left-half blue and right-half red circle versus red diamond). In contrast, adding shallow convection in the extratropics in both hemispheres shifts the jet back to its control position (Fig. 5e, left-half red and right-half blue circle versus blue diamond). This suggests that, in DJF, the impact of shallow convection on the position of the jet occurs largely due to its presence in the midlatitudes, rather than the tropics. Further constraining shallow convection in the midlatitude to only one hemisphere, and to middle versus high latitudes, shows that, in DJF, the difference in jet position is attributed to shallow convection in the southern midlatitudes between 20° and 50°S. Enabling shallow convection only in this latitude band in the SH produces the same jet position as the Control (Fig. 7a, red–blue upward triangle).

The picture appears quite different in JJA. In this season, we saw that the difference between the Only-Deep and Only-Shallow configurations spanned a smaller portion of the AMIP spread (Fig. 5f, red and green diamonds). Further insight is achieved in this case by turning convection off entirely either in the tropics or extratropics (Figs. 5e,f, red and green half empty circles). For example, disabling all convective parameterization in the extratropics while keeping Only-Deep in the tropics results in a 3.5° equatorward shift compared to keeping deep convection on everywhere (Fig. 5f, left red and right empty circle). The opposite shift occurs if convective parameterization is disabled entirely in the tropics (Fig. 5f, red empty circle). A similar behavior is seen when the Only-Shallow configuration is used in the tropics or extratropics and convective parameterization is entirely disabled everywhere else (green empty circles). This shows that in CAM4, in JJA, the contribution of convective parameterization to the position of the jet differs from DJF. In JJA, it appears that the position of the jet is a combination of opposite tropical and extratropical influences.

Finally, in terms of the global mean budget, we note that both the Conv-Off and Only-Deep configurations produce similar, and substantial, net energy loss at the top of the atmosphere (TOA), with annual average net loss greater than 30 W m^{-2}, as compared with near balance (as expected) in the Control configuration. The imbalances are explained by excess low cloud in the absence of shallow convection. Yet these configurations are at the two opposite extremes of jet positions in the CAM ensemble (Figs. 5e,f, red and empty diamonds). Also, as noted earlier, zonal-mean radiative variables are moderately correlated with the spread of jet positions in the AMIP ensemble (Fig. S1). This suggests that other aspects of convective parameterization, such as latitudinal variations in atmospheric heating, are a more plausible mechanism in explaining intermodel differences in jet positions.

5. Hypotheses linking convective and jet biases

The midlatitude jet is often thought of as a by-product of equator-to-pole temperature imbalance (Wilcox et al. 2012; Butler et al. 2011, 2010). For example, Butler et al. (2010) study the jet response to tropical upper-tropospheric warming that is expected as a result of an increase in greenhouse gas concentrations. This is of interest since much of this warming pattern is in response to increased latent heating from moist processes, and therefore it is natural to try and fit differences in parameterization of moist convection into the same framework. However, we do not find strong correlation between jet positions in the AMIP ensemble and seasonal temperature differences between the tropics and the pole [see Eq. (2)]. This was reinforced in section 4, which suggested that differences in parameterization of convection in the midlatitudes play a role in the spread of SH jet positions in AMIP. It highlighted differences in the amount of shallow convection that models produce in the midlatitudes as a potential factor in this spread.

In DJF, we find that SH jet positions in the AMIP ensemble are correlated with SH midlatitude tropospheric column average lapse rate (Γ_{ML}), averaged between 925 and 300 hPa and over 20°–50°S (Fig. 5c; $r = -0.81$). The chosen spatial and vertical extents in Fig. 5 are set to match the covariances of temperature with jet positions seen in Figs. 1 and 2. The correlation is qualitatively insensitive to the latitudinal extent within the midlatitudes. It is also strong when only models from the CMIP6 ensemble are included (Figs. S4–S6). The relationship to Γ_{ML} weakens in JJA (Fig. 5d; $r = -0.51$). It is also weaker in the ocean–atmosphere coupled scenario (Figs. 5a,b), suggesting that ocean variability is somehow contributing to the spread independently of Γ_{ML}, especially in winter.

The slope of the line of best fit between Γ_{ML} and jet positions in AMIP is qualitatively reproduced by the Only-Deep, Only-Shallow, and Control CAM4 configurations (Figs. 5e,f). Especially in DJF, differences in tropical shallow convection explain most of the Γ_{ML} differences between the Only-Deep and Control CAM4 configurations (Fig. 5e, blue–red circle vs red diamond). Conversely, enabling shallow convection in the extratropics only shifts the jet poleward back to the Control configuration, with only a small decrease in Γ_{ML} (Fig. 5e, red–blue circle vs red diamond).

We seek to constrain the set of mechanisms by which midlatitude shallow convection can shift the jet. To this end, we follow Shaw (2019), who lists 18 mechanisms that can explain the shift of the zonal-mean midlatitude circulation in response to an increase in carbon dioxide levels. Our assumption is that these mechanisms are also applicable to a perturbed physics scenario that originate from parameterization of shallow convection. By way of elimination, we rule out mechanisms that did not originate in the midlatitudes, or that involve SST differences. We also rule out mechanisms that did not show high correlation with the spread of jet positions, such as radiative effects (Fig. S1) and effects of convection on tropopause height (not shown). Some mechanisms related to Hadley cell expansion involve extratropical eddies (e.g., Staten et al. 2018) and therefore are convolved with mechanisms related to the position of the midlatitude jet that will be discussed shortly. However, our experiments where convection has been altered in restricted latitude bands showed tropical heating to be less important in explaining the differences in jet positions in DJF. We are left with two mechanisms related to increased dry static stability in the midlatitudes (i.e., Frierson

2008; Kidston et al. 2011), and one mechanism related to increased specific humidity [Held 2015; see further discussion in Shaw (2019)].

Kidston et al. (2011) argues that an increase in dry static stability in the midlatitudes increases the Rossby radius of deformation, causing eddies to dissipate farther poleward, thus shifting the jet. Since the introduction of shallow convection in the midlatitudes in DJF decreases Γ_{ML} (Fig. 5e, blue vs red diamonds), this can explain the tendency of CAM4 to move the jet poleward when shallow convection is enabled in the midlatitudes. As opposed to the scenario discussed by Kidston et al., here the increase in static stability is confined both seasonally and to the hemisphere where shallow convection is prevalent. Since this mechanism does not directly involve moist dynamics, and noting that shallow convection is prevalent throughout the SH midlatitudes (Figs. 3h and 4h), we conduct additional simulations where shallow convection is replaced with a heat patch of 2.0×10^{-3} J kg^{-1} s^{-1} between sigma levels 929–600 and latitudes 20°–50° in both hemispheres. This approach is valid if the added heating does not significantly affect other processes that can shift the jet. This heating patch was sufficient to shift the jet from the initial CAM4 Only-Deep configuration most of the way back to the position in the Control configuration (Fig. 7a, right half orange, left half red square markers). However, the heating did not alter the average Γ_{ML}. Moreover, a greater change to Γ_{ML} is seen when adding the heat patch in the tropics between 20°S and 20°N, but this has a smaller effect on jet position (Fig. 7a, right half red, left half orange square markers). This is consistent with the experiment where shallow convection was enabled in the tropics or extratropics (Fig. 7a, blue–red vs red–blue circles, respectively). We thus infer that direct heating by shallow convection is a plausible mechanism, but the gross Γ_{ML} is not a good representative of that mechanism.

Next, we note that the mechanisms proposed by Frierson (2008) and Held (2015) both originate in latitudinal asymmetries of water vapor increases and share a common source, where the authors studied the effects of water vapor increases on circulation (Frierson et al. 2006, 2007, hereafter FHZ06 and FHZ07). Frierson (2008) and FHZ07 argue that the increase in water vapor on the equatorward flank of the storm tracks increases dry static stability in this region and in turn reduces eddy generation. This leads to an equatorward momentum flux and in turn a poleward jet shift (see also Shaw 2019, and the Fig. 2 scenario 2 therein). We note that in the SH DJF, this argument can apply to the AMIP ensemble, as well as to the convection on–off experiments with CAM4. In AMIP, models with a poleward jet position show lower EKE in the lower midlatitudes when compared to models with a more equatorward jet position (Fig. 6a). This is matched by higher degree of specific humidity in this region for models with a more poleward jet position (Fig. 6c), and a poleward shift in temperature gradient maxima in accordance with Frierson (2008) and FHZ07 (Fig. 6g). Consistent with the argument presented by Frierson (2008), maximum temperature gradients appear poleward in models that are moister in the lower midlatitudes. In CAM4, the increase in specific humidity arises from the introduction of shallow convection into the Only-Deep configuration (Fig. 6c, dashed vs dash–dotted lines), which is adjoined by a reduction of EKE (Fig. 6a).

While the hypothesis proposed by Frierson (2008) aligns remarkably well with both the AMIP ensemble and CAM4 in DJF, the hypotheses of Held (2015) may also apply to this season. Held (2015) proposes the idea that an increase in water vapor around the storm tracks make the storms more efficient in transporting energy. Since the increase in water vapor is greater at the equator side of the storm tracks' maximum activity, it is balanced by a poleward shift of the storm tracks. We note that for AMIP, the correlation between specific humidity and EKE and jet positions in DJF peaks at the lower midlatitudes (Fig. 6a, vertical line). In accord with Held (2015), in this season AMIP models with a more poleward jet position tend to precipitate more equatorward from 35°S, especially to the east of continents (Fig. 3e). As noted earlier, this is dominated by convective precipitation. Interestingly, the increase in precipitation covariance with the jet equatorward from 35°S is matched by negative covariance poleward from this latitude (Fig. 3e). In CAM4, this is marked by a transition from deep convection in the Only-Deep configuration to shallow convection in the Control configuration (Figs. 3f,h,j). In DJF, AMIP models with a more poleward jet position also tend to show a higher gradient of specific humidity, peaking at 0.3 g kg^{-1} per degree in the midlatitudes around 35°S where the correlation of specific humidity gradients with the jet maximizes (Fig. 6e). In Fig. 6e the presence of an independent shallow convection scheme in CAM4 (dashed line) reproduces the peak in moisture gradients in AMIP, while the exclusion of shallow convection (dash–dotted line) flattens this gradient, making it more meridionally homogeneous. This supports the idea that the ability of AMIP models to moisten the lower midlatitudes is key to explaining the spread of jet positions in AMIP.

One way to increase our confidence in the applicability of the mechanisms proposed by Frierson (2008) and Held (2015) is to enable shallow convection in narrow latitudinal bands across the midlatitudes. If the contribution of shallow convection to jet position is solely due to moistening at the equatorward flank of the storm tracks, one would expect activation of shallow convection at higher midlatitudes not to contribute to the jet position. To this end, shallow convection is introduced to the Only-Deep CAM4 configuration in narrow bands at 20°–50°S, 20°–30°S, 30°–40°S, and 40°–50°S (Fig. 7, triangles). As mentioned earlier, in DJF, enabling shallow convection between 20° and 50°S brings the jet position to the location of the Control configuration (Fig. 7a, red–blue up triangle). In both seasons, the contribution of the three latitudinal subbands seems to additively contribute to the CAM4 Control jet position, with the largest contribution coming from the 30°–40°S band. In DJF, the contribution from the 40°–50°S band seems negligible (Fig. 7a, red–blue right triangle), in line with the hypotheses proposed by Frierson (2008) and Held (2015).

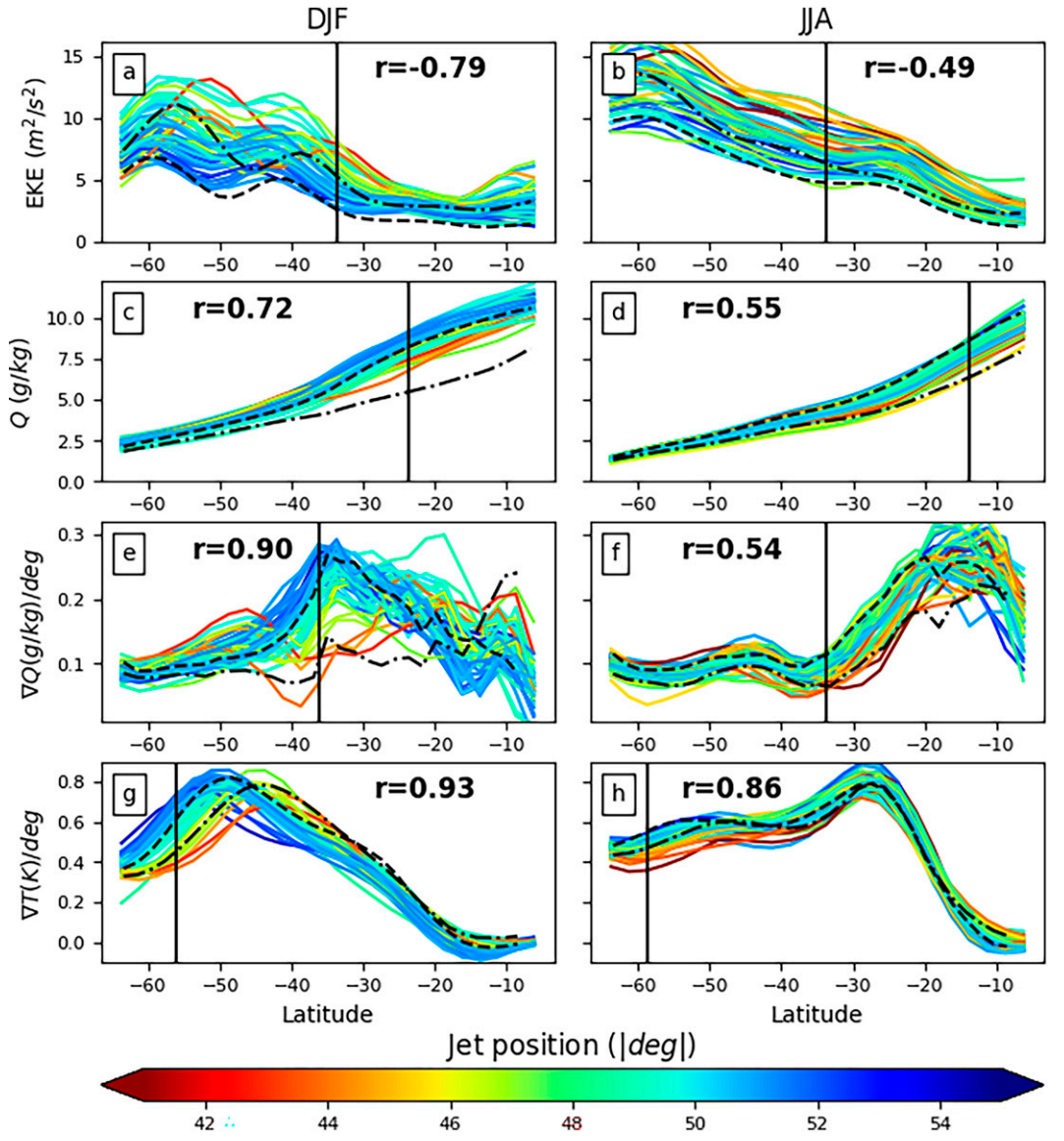

FIG. 6. (from top to bottom) Poleward EKE at 600 hPa, zonal-mean specific humidity, specific humidity meridional gradients at 850 hPa, and temperature meridional gradients at 600 hPa in the AMIP ensemble and CAM4. Specific humidity is sampled at 850 hPa, which is roughly at the level of maximum correlation with the jet (Figs. 1 and 2e,f). Color scale denotes jet position with more poleward (equatorward) jet position in blue (red). Gradients are calculated per degree south. CAM Control and Only-Deep configurations are marked by dashed and dash–dotted black lines. The latitude of maximum correlation with jet positions is denoted by black vertical lines with the correlation coefficient printed next to it.

6. A classification of climate models

The results so far attribute much of the spread of model jet positions in DJF to the treatment of shallow convection. However, this was achieved using a single model. It is therefore tempting to classify atmospheric models based on their parameterization of convection and match it to the spread of jet positions in the AMIP ensemble. Parameterization of convection in models is complex and varied, making this a challenging and subjective exercise. Previous sections identified a competition between deep and shallow convection in the midlatitudes as a key process modulating moistening and heating with a knock-on effect on the position of the jet.

Following this reasoning, a subset of models in the AMIP ensemble is classified into two groups (Table 2; see also Table S1 in the online supplemental material): Group A is composed from models with a convection scheme where shallow convection can independently evolve, while for group B models it does not. The classification process followed a set of guidelines: models in group A were those for which the models' documentation mentioned independent features

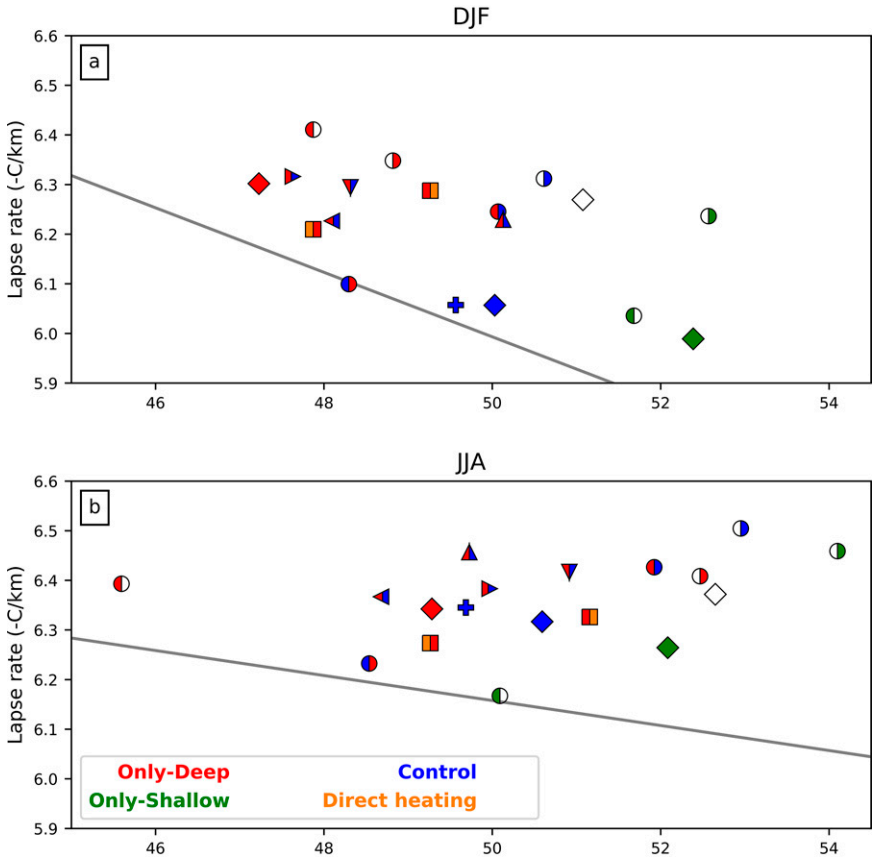

FIG. 7. Relationship between midlatitude lapse rate (Γ_{ML}) and SH jet position in CAM4. Red, green, blue, and empty shapes mark Only-Deep, Only-Shallow, Control, and Conv-Off configurations, respectively. Diamond markers denote the base CAM4 configurations, while left (right) color marks the configuration that is applied inside (outside) latitudes 20°S–20°N (see also Table 1 and Figs. 5e,f). Orange color marks an Only-Deep CAM4 configuration with tropospheric heat patch of 2.0×10^{-3} J kg^{-1} s^{-1} along 20°S–20°N and between sigma levels 929–192 (left orange, right red square), and outside 20°S–20°N and between sigma levels 992–600 (left red, right orange square). Triangles mark shallow convection enabled in the SH only between latitudes 20°–50°S (up), 20°–30°S (left), 30°–40°S (down), 40°–50°S (right) showing that the contribution of shallow convection to jet shift is a sum of all midlatitude bands. A blue plus marker denotes an additional CAM4 configuration where shallow convection is disabled northward of 20°N. A gray line marks the line of best fit in AMIP (see Figs. 5c,d).

of shallow convection. For example, the convection the GFDL-HIRAM-C180 was implemented using Bretherton et al. (2004), which is a shallow convection scheme. The same scheme was used in GFDL CM3 as the shallow convection scheme that independently coexisted alongside a deep convective scheme (Donner et al. 2011, as well as in later versions of CAM). Another example is HadGEM2 (Martin et al. 2011), where specific features were added, allowing additional

TABLE 2. Classification of AMIP models based on their treatment of shallow and deep convection.

Group	Main partition	Subgroup	Description
A	Independent shallow convection	Simultaneous	Shallow convection is calculated independently from deep convection
		Only-Shallow	Deep convection is disabled (currently including the GFDL-HIRAM-C180 only)
B	Unified or no shallow convection	Bulk	Models in this class descend from the bulk approach of Tiedtke (1989)
		Unified	Models in this class descend from the unified approach of Arakawa and Schubert (1974) or buoyancy sorting scheme of Emanuel (1991)
		Only-Deep	Only deep convection is implemented

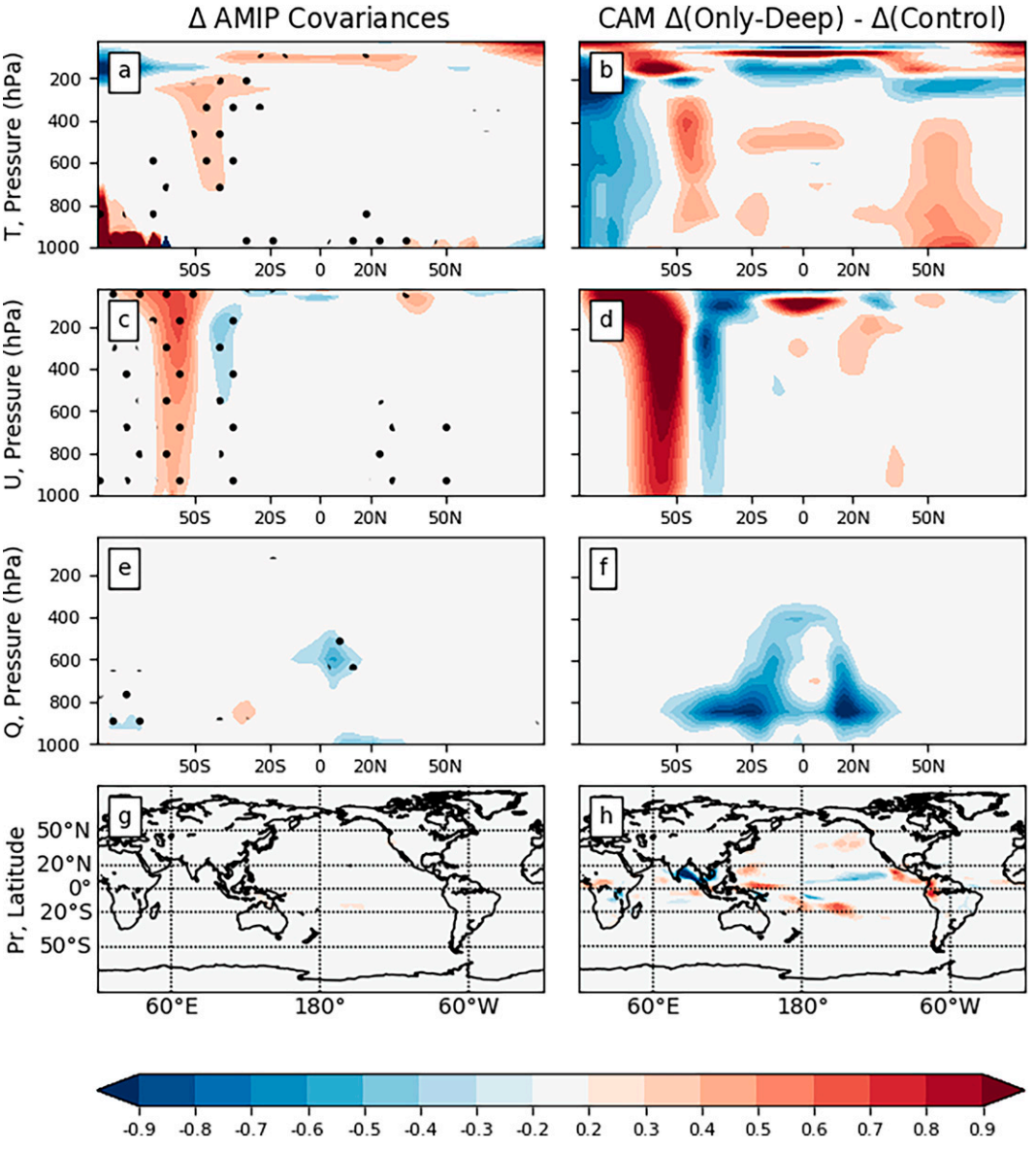

FIG. 8. Relationship between SH jet shift and changes to variables in the AMIP+4K ensemble and in CAM in DJF. (left) Covariances of changes in AMIP and (right) differences of changes of CAM4 Only-Deep minus Control configurations (representing large and small jet shifts, respectively). Rows show (from top to bottom) zonal-mean temperature (0.5 × K × degrees south), zonal wind speed (m s^{-1} × degrees south), specific humidity (0.25 × g kg^{-1} × degrees south), and precipitation (2.0 × mm day^{-1} × degrees south). Stippling in the left column denotes significance at the 95% confidence interval ($|r| > 0.3$ assuming an independent sample). The left and right columns use equivalent scales.

degrees of freedom in representing shallow convection. Some models adopted complete implementations of other models or their convection schemes. Where it was clear from the documentation that these models are based on a model in group A, these were also added to the group. For example, the atmospheric component of NorESM1-M and Can-AM4 are derivatives of CAM.

Models in group B presented a greater challenge, since in general in this group a single convective scheme implemented both deep and shallow convection and the associated documentation did not directly discuss shallow convection. For this group we relied on the theoretical origins of the implementation of their convective parameterization. For example, models where the convection scheme descends from Arakawa and Schubert (1974), such as MIROC5, parameterize a theoretical ensemble of plumes to a single unified profile. These implementations passed many cycles of improvements from their theoretical origin, which is likely to result in a larger spread in this group. Moreover, in some models the convection scheme offers innovative features that go beyond their

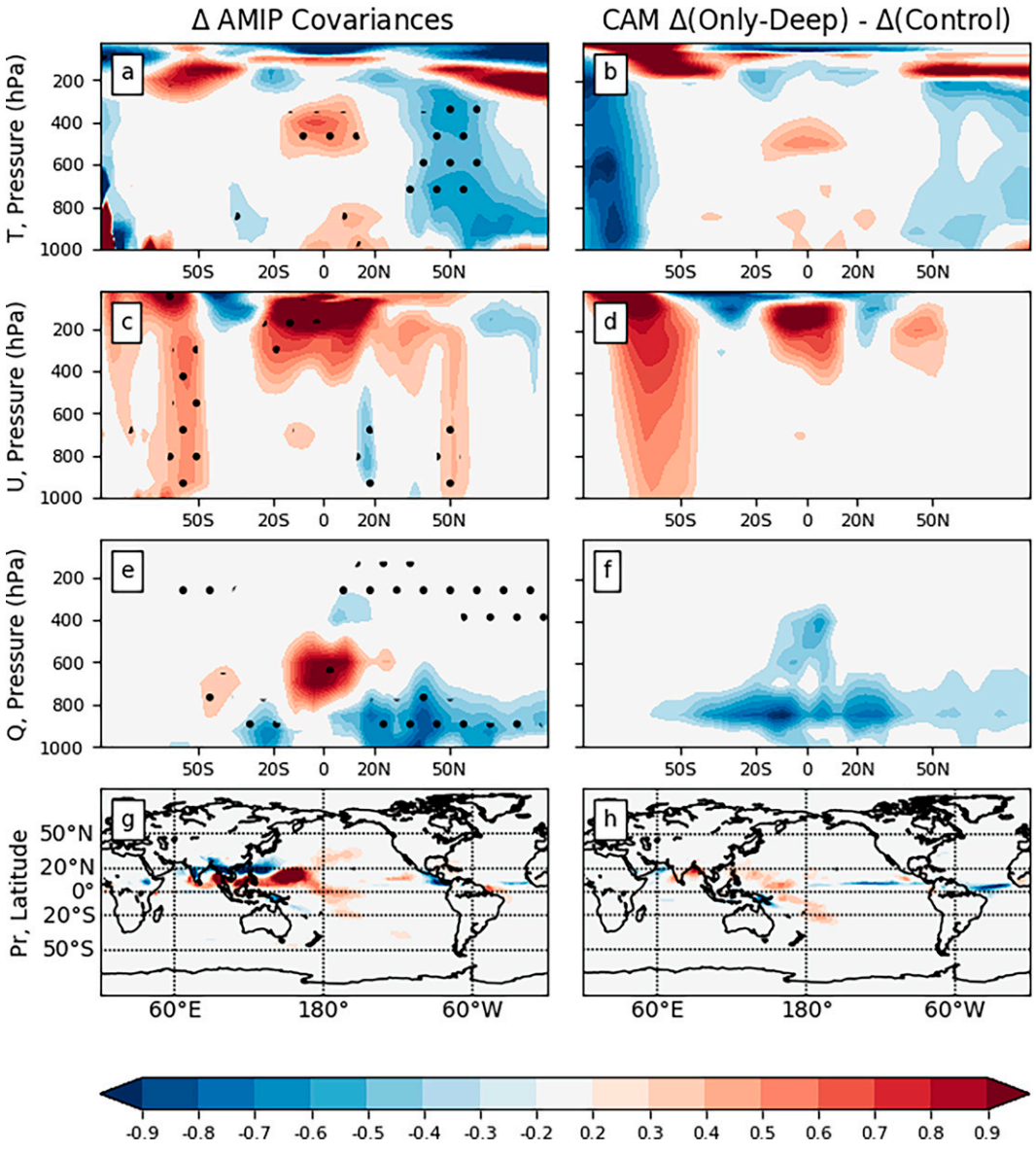

FIG. 9. As in Fig. 8, but for JJA.

theoretical origin. For example, IPSL-CM5B-LR includes a novel parameterization of convective cold pools. This idea goes considerably beyond its theoretical origins and is likely to be in a class of its own. These cases, where the model's documentation was reviewed but we failed to classify the model to one of the two groups, are listed in Table S1 but are labeled as "unclassified."

To explain some of the variability in each group, the groups are further divided to subgroups. Group A is subdivided to the Only-Shallow subgroup, where a shallow convective parameterization is used for all convection, and Simultaneous, where, as in CAM4, shallow convection is activated independently from deep convection, or specific features are in place allowing additional degrees of freedom in representing shallow convection (e.g., Martin et al. 2011). Group B is composed of the Unified, Bulk, and Only-Deep subgroups. Parameterizations in the Unified class descend from the unified approach of Arakawa and Schubert (1974) or from density function–based parameterizations of Emanuel (1991). Parameterizations in the Bulk class descend from the bulk approach of Tiedtke (1989). Broadly, models in group B tend to select a joint shallow or deep convective representation at each grid point and time step, while group A tends to allow shallow and deep convection to evolve more independently (see also Table 2).

This yields 16 models that are classified (Table S1), providing a good coverage of the spread of jet positions in the AMIP ensemble. Figures 5a–d show that models in group A tend to have a more poleward biased jet position. As expected, group B exhibit a wider spread of jet positions and tend to be at the equatorward flank of the ensemble. We also note

the alignment between this classification and the CAM4 ensemble. For example, in Fig. 5c and Table S2, GFDL-HIRAM-C180, being the only model in the Only-Shallow subgroup, is at the poleward and moister part of the ensemble (green diamond), while CNRM-CM5, which is the only model in the Only-Deep subgroup, is at the drier equatorward part of the ensemble (red diamond). Another example is MPI-ESM-MR, which belongs to the Bulk group, having a drier equatorward position in DJF. We also note that in AMIP at the poleward extreme of the spread of jet positions we find models from group A, while at the equatorward extreme we find models from group B (Figs. 5c,d). Although not a strong test of the applicability of insights from the CAM4 configurations to the AMIP ensemble, these results appear consistent with the idea that convective schemes play a significant role in the spread of jet positions.

7. Climate warming scenario

Jet shifts in response to global warming have been associated with warming in the tropical upper troposphere (Butler et al. 2010). It has been suggested that these jet shifts are mediated by eddy–mean state feedback (Butler et al. 2011), with the larger shifts also associated with a more persistent Southern Annular Mode (Kidston and Gerber 2010). The latter mechanism has been of interest since it implies a way by which future jet shifts can be constrained by knowledge of today's climate. Yet, for unknown reasons, this relation was found to be seasonal, showing high significance in JJA and low in DJF (see correlations in Figs. 11a and 11b), which cannot be explained by these mechanisms (Simpson and Polvani 2016).

We seek to understand the ways by which intermodel differences in convective parameterizations might contribute to the spread of jet shifts in a warmer climate. In both DJF and JJA we do not find that the mechanisms proposed in section 5 based on state differences in the SH midlatitudes successfully explain the spread in jet shifts. Neither midlatitude temperature changes nor the changes in specific humidity in the SH covary significantly with jet shifts (Figs. 8 and 9, left). In JJA, correlations with temperature changes are found in the tropical upper troposphere and the Northern Hemisphere (NH) midlatitudes and are matched by lower tropospheric changes of specific humidity. Figure 9 (right) show the differences in warming-induced atmospheric changes in CAM4 between the Only-Deep and Control configurations. The CAM4 differences are on par with the covariances seen in the AMIP ensemble, with greater NH midlatitude warming and moistening for smaller jet shifts and greater tropical upper-tropospheric warming for larger jet shifts. We note that, while encouraging, these CAM4 configurations account for 1° of jet shift compared to 4.5° in the AMIP ensemble.

These results suggest two hypotheses for a relationship between convection and biases in jet shift in JJA:

1) Tropical influence
   The same biases in convective parameterization that lead to intermodel differences in midlatitude moisture work more effectively in the tropics in a climate warming scenario. For example, through intermodel spread of magnitude and shape of upper-tropospheric warming (Butler et al. 2010), or through the differences in local and global mixing (Sherwood et al. 2014; Watt-Meyer and Frierson 2019). This is supported by the co-occurrence of tropical moisture increases matched by tropical upper-tropospheric warming and tropical precipitation changes (Figs. 9a,g).
2) Opposite hemisphere (NH) influence
   This hypothesis follows the idea that the same biases in parameterization of shallow convection that were found in the SH summer would also be found in the NH summer. These may affect the SH jet via interhemispheric teleconnections (Ceppi et al. 2013). Briefly, Ceppi et al. (2013) show that the jet in one hemisphere can respond to a thermal forcing in the opposite hemisphere through dynamical interhemispheric teleconnections. In this framework, a warming confined to one hemisphere intensifies the Hadley cell in the opposite hemisphere, strengthening the subtropical jet and, in turn, pulling the midlatitude jet equatorward. Indeed smaller SH jet shifts tend to covary with warming and larger moistening of the NH midlatitudes (Figs. 9a,e).

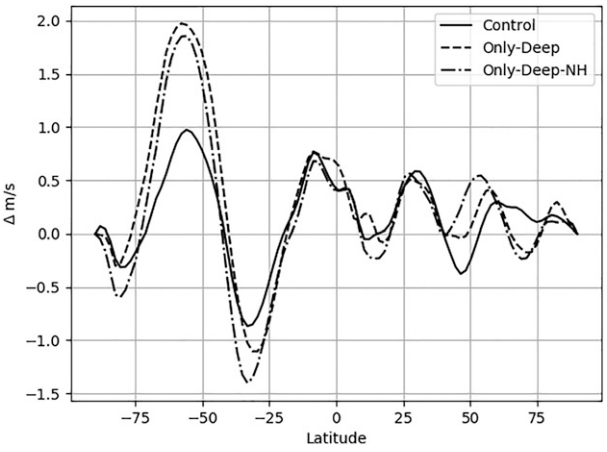

FIG. 10. Zonal-mean zonal wind changes in AMIP+4K CAM4 during JJA. The Only-Deep-NH configuration denotes a CAM4 configuration where shallow convection is disabled poleward of 20°N.

To test these two possibilities, we conduct further experiments with CAM4 where a +4 K SST perturbation is added. First, shallow convective parameterization is disabled in the tropics between 20°S and 20°N. This did not change the jet shift, leaving it at the same magnitude as the Control configuration. Second, shallow convective parameterization is disabled northward from 20°N. This qualitatively reproduces the poleward drying and cooling pattern in the NH midlatitudes, associated with a poleward SH jet shift during JJA as seen in AMIP (Figs. 9a,e) and in CAM4 (Figs. 9b,f). SH midlatitude zonal wind speed changes with warming, in this case, closely follow the changes seen in the Only-Deep CAM4 configuration despite having the Control configuration throughout the SH midlatitudes and the tropics (Fig. 10).

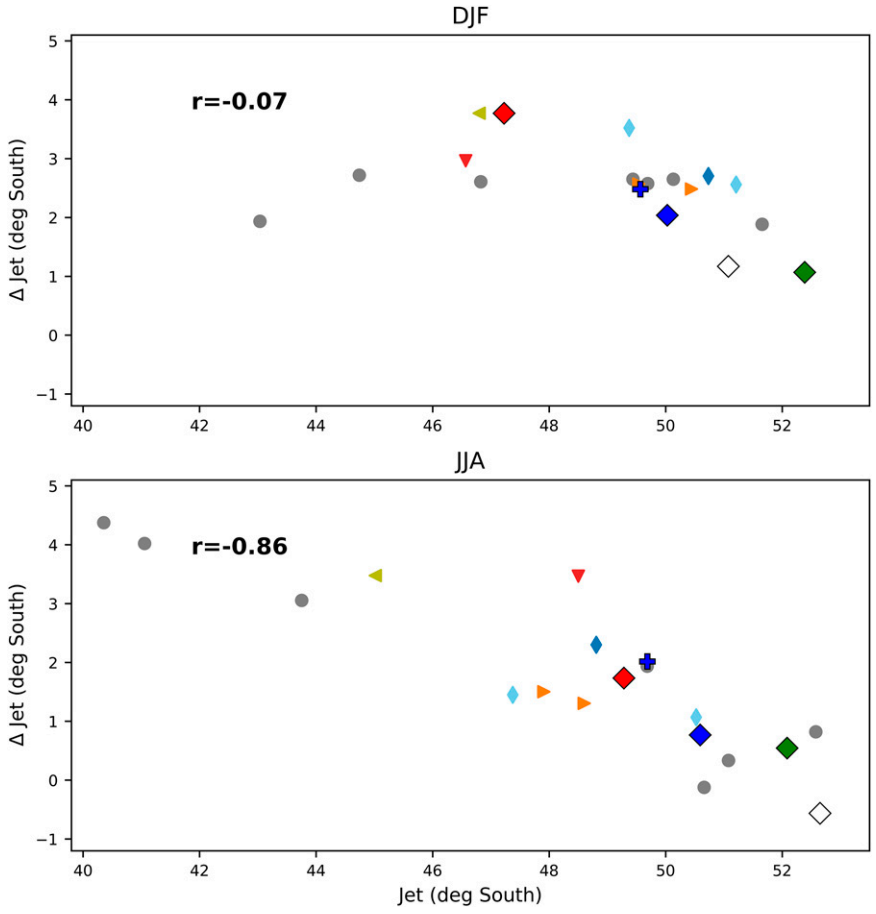

FIG. 11. SH jet position in AMIP and CAM4 vs jet shift in AMIP+4K scenario, for (top) summer and (bottom) winter. Markers and colors are as in Fig. 5 and Tables 1 and 2. Small markers denote AMIP models; as in Figs. 5a–d, blue and light blue markers denote group A models, and gray circles denote unclassified models. Large diamonds mark the base CAM4 configurations (Table 1 and Figs. 5e,f). A blue plus marker denotes an additional CAM4 configuration where shallow convection is disabled northward of 20°N. The correlation is displayed in the upper left and includes only AMIP models.

Crucially, disabling shallow convection in the NH sets the jet's initial position and shift in JJA to the same location as the Only-Deep configuration (Fig. 11b), while in DJF both jet position and shift match the CAM4 Control configuration (Fig. 11a). This is consistent with the fact that convective parameterization in the SH matches the Control configuration. It suggests that as opposed to DJF, in JJA both the SH jet position and shift in a warmer climate are affected by the amount of shallow convection that is present in the NH midlatitudes. Thus, in accordance with Ceppi et al. (2013), shallow convection produces stronger warming in the NH midlatitudes when compared to cases that lack shallow convection, resulting in a smaller jet shift in the opposite hemisphere (SH).

8. Conclusions

This study provides compelling evidence that midlatitude moist convection plays an important role in modulating the position of the SH midlatitude jet in present climate and its shift as the climate warms. Atmospheres that lack shallow convection in the lower midlatitudes tend to position the summertime jet closer to the equator. Latitude-restricted, convection on–off experiments with CAM4 show that difference in the amount of deep and shallow convection in the midlatitudes region can account for 60% of the summertime spread of jet positions in the AMIP ensemble, encompassing all but four of the models.

The impact of this mechanism on intermodel spread is less pronounced in winter, where models exhibit a smaller spread of lower-tropospheric moisture in the SH midlatitudes. Instead, our results suggest that the same mechanism is at play in the NH, affecting the SH jet via interhemispheric teleconnections. This is seen especially in the covariances of SH jet shift with changes in temperature and moisture in a warmer climate, where significant correlations appear in the NH midlatitudes. In line with these, in CAM4

we find that, by disabling shallow convection in the NH poleward from 20°N, the model exhibits SH jet position and shift that follow the CAM4 Control configuration in DJF and the Only-Deep configuration in JJA. While these changes are small compared to the overall spread in AMIP, they follow the relation between jet position and shift.

Shallow convection in the midlatitudes affects the jet by locally moistening and warming the upper troposphere. A plausible mechanism is that while deep convective schemes typically bring cold and dry air into the planetary boundary layer (PBL) via downdrafts, shallow convection can generate rain without doing as much of this, hence producing a mean state with higher moist enthalpy in the PBL, a warmer moist adiabat, and a warmer troposphere aloft via interaction with deep convection and large-scale ascent—a mechanism analogous to "turbo charging." Indeed, by disabling shallow convective parameterization and comparing it to the default "Control" configuration in CAM4 we were able to qualitatively reproduce the covariance of the jet with many important variables such as temperature, specific humidity, and precipitation. We proposed three hypotheses from current literature by which shallow convection can shift the jet, and offer ways to test them. In DJF, enabling shallow convection in the lower SH midlatitudes (20°–40°S) dominates the change in jet position compared to higher midlatitudes. Interestingly, in DJF, both AMIP and our experiments with CAM4 align remarkably well with the hypothesis made by Frierson (2008) and FHZ07, showing a reduction in EKE proportional to moistening of the lower midlatitudes, and a matching poleward shift in the maxima of zonal-mean temperature gradients. However, this is not sufficient to disprove the other two hypotheses.

The tropical troposphere plays a smaller role than the midlatitudes in the AMIP intermodel spread. The tropics tend to be warmer when shallow convection is present, presumably because the same convective processes operate globally, with CAM4 experiments showing an increase in tropical deep convective precipitation, and a decrease in the subtropics, when shallow convection is present. Furthermore, the relative roles of deep convection versus large-scale condensation and interaction between convective parameterization and microphysical parameterization require further study and could be important in determining spread of jet positions. In CAM4, removing parameterized convection entirely results in a jet poleward from its control configuration. We also note that the combination of deep and shallow convective parameterization in CAM4 tends to suppress deep convection in the midlatitudes, closer to the jet, potentially increasing the asymmetry in warming on the equatorward side of the storm tracks—in accordance with the mechanism proposed in Held (2015). We also notice a potential relation to ocean–land interactions, seen in the relation between jet position and convective precipitation east of continents in DJF. This may also play a role in intermodel differences in midlatitude cooling in the NH summer. This work focused on the AMIP scenario where all the models use the same fixed SST, placing models at a level playing field. It is noted that SST-related mechanisms can be of primary importance in determining the jet position in an ocean–atmospheric coupled configuration.

Our study has shown that small-scale convective processes, which are already important to many other aspects of weather and climate but are traditionally thought to matter little outside the tropics, play an unexpectedly strong role in determining the latitude of midlatitude jets and weather systems. Improved understanding of, and ability to model, these processes appear necessary to pin down how midlatitude weather will be affected by global warming.

Acknowledgments. UCAR and NCAR, in the United States, are acknowledged for making CESM model code available at the public Subversion code repository (http://www.cesm.ucar.edu/models/cesm1.0/). The computational support was provided by NCI and CMS team at CCRC. SCS, DF, and VD were supported by Australian Research Council Grant FL150100035.

Data availability statement. The data that support the findings of this study are available on request from the corresponding author.

REFERENCES

Arakawa, A., 2004: The cumulus parameterization problem: Past, present, and future. *J. Climate*, **17**, 2493–2525, https://doi.org/10.1175/1520-0442(2004)017<2493:RATCPP>2.0.CO;2.

——, and W. H. Schubert, 1974: Interaction of a cumulus cloud ensemble with the large-scale environment, Part I. *J. Atmos. Sci.*, **31**, 674–701, https://doi.org/10.1175/1520-0469(1974)031<0674:IOACCE>2.0.CO;2.

Armour, K. C., J. Marshall, J. R. Scott, A. Donohoe, and E. R. Newsom, 2016: Southern Ocean warming delayed by circumpolar upwelling and equatorward transport. *Nat. Geosci.*, **9**, 549, https://doi.org/10.1038/ngeo2731.

Barnes, E. A., and L. Polvani, 2013: Response of the midlatitude jets, and of their variability, to increased greenhouse gases in the CMIP5 models. *J. Climate*, **26**, 7117–7135, https://doi.org/10.1175/JCLI-D-12-00536.1.

——, N. W. Barnes, and L. M. Polvani, 2014: Delayed Southern Hemisphere climate change induced by stratospheric ozone recovery, as projected by the CMIP5 models. *J. Climate*, **27**, 852–867, https://doi.org/10.1175/JCLI-D-13-00246.1.

Bony, S., M. Webb, C. Bretherton, S. Klein, P. Siebesma, G. Tselioudis, and M. Zhang, 2011: CFMIP: Towards a better evaluation and understanding of clouds and cloud feedbacks in CMIP5 models. *CLIVAR Exchanges*, No. 56, International CLIVAR Project Office, Southampton, United Kingdom, 20–22.

Bracegirdle, T. J., E. Shuckburgh, J.-B. Sallee, Z. Wang, A. J. S. Meijers, N. Bruneau, T. Phillips, and L. J. Wilcox, 2013: Assessment of surface winds over the Atlantic, Indian, and Pacific Ocean sectors of the Southern Ocean in CMIP5 models: Historical bias, forcing response, and state dependence. *J. Geophys. Res. Atmos.*, **118**, 547–562, https://doi.org/10.1002/jgrd.50153.

Brayshaw, D. J., B. Hoskins, and M. Blackburn, 2008: The storm-track response to idealized SST perturbations in an aquaplanet GCM. *J. Atmos. Sci.*, **65**, 2842–2860, https://doi.org/10.1175/2008JAS2657.1.

Bretherton, C. S., J. R. McCaa, and H. Grenier, 2004: A new parameterization for shallow cumulus convection and its application to marine subtropical cloud-topped boundary layers. Part I: Description and 1D results. *Mon. Wea. Rev.*, **132**, 864–882, https://doi.org/10.1175/1520-0493(2004)132<0864:ANPFSC>2.0.CO;2.

Butler, A. H., D. W. J. Thompson, and R. Heikes, 2010: The steady-state atmospheric circulation response to climate change–like thermal forcings in a simple general circulation model. *J. Climate*, **23**, 3474–3496, https://doi.org/10.1175/2010JCLI3228.1.

——, ——, and T. Birner, 2011: Isentropic slopes, downgradient eddy fluxes, and the extratropical atmospheric circulation response to tropical tropospheric heating. *J. Atmos. Sci.*, **68**, 2292–2305, https://doi.org/10.1175/JAS-D-10-05025.1.

Ceppi, P., and D. L. Hartmann, 2013: On the speed of the eddy-driven jet and the width of the Hadley cell in the Southern Hemisphere. *J. Climate*, **26**, 3450–3465, https://doi.org/10.1175/JCLI-D-12-00414.1.

——, Y.-T. Hwang, X. Liu, D. M. W. Frierson, and D. L. Hartmann, 2013: The relationship between the ITCZ and the Southern Hemispheric eddy-driven jet. *J. Geophys. Res. Atmos.*, **118**, 5136–5146, https://doi.org/10.1002/jgrd.50461.

——, M. D. Zelinka, and D. L. Hartmann, 2014: The response of the Southern Hemispheric eddy-driven jet to future changes in shortwave radiation in CMIP5. *Geophys. Res. Lett.*, **41**, 3244–3250, https://doi.org/10.1002/2014GL060043.

——, D. L. Hartmann, and M. J. Webb, 2016: Mechanisms of the negative shortwave cloud feedback in middle to high latitudes. *J. Climate*, **29**, 139–157, https://doi.org/10.1175/JCLI-D-15-0327.1.

Davis, S. M., and K. H. Rosenlof, 2012: A multidiagnostic intercomparison of tropical-width time series using reanalyses and satellite observations. *J. Climate*, **25**, 1061–1078, https://doi.org/10.1175/JCLI-D-11-00127.1.

Dee, D. P., and Coauthors, 2011: The ERA-Interim reanalysis: Configuration and performance of the data assimilation system. *Quart. J. Roy. Meteor. Soc.*, **137**, 553–597, https://doi.org/10.1002/qj.828.

Donner, L. J., and Coauthors, 2011: The dynamical core, physical parameterizations, and basic simulation characteristics of the atmospheric component AM3 of the GFDL global coupled model CM3. *J. Climate*, **24**, 3484–3519, https://doi.org/10.1175/2011JCLI3955.1.

Emanuel, K. A., 1991: A scheme for representing cumulus convection in large-scale models. *J. Atmos. Sci.*, **48**, 2313–2329, https://doi.org/10.1175/1520-0469(1991)048<2313:ASFRCC>2.0.CO;2.

Eyring, V., S. Bony, G. A. Meehl, C. A. Senior, B. Stevens, R. J. Stouffer, and K. E. Taylor, 2016: Overview of the Coupled Model Intercomparison Project Phase 6 (CMIP6) experimental design and organization. *Geosci. Model Dev.*, **9**, 1937–1958, https://doi.org/10.5194/gmd-9-1937-2016.

Frierson, D. M. W., 2008: Midlatitude static stability in simple and comprehensive general circulation models. *J. Atmos. Sci.*, **65**, 1049–1062, https://doi.org/10.1175/2007JAS2373.1.

——, I. M. Held, and P. Zurita-Gotor, 2006: A gray-radiation aquaplanet moist GCM. Part I: Static stability and eddy scale. *J. Atmos. Sci.*, **63**, 2548–2566, https://doi.org/10.1175/JAS3753.1.

——, ——, and ——, 2007: A gray-radiation aquaplanet moist GCM. Part II: Energy transports in altered climates. *J. Atmos. Sci.*, **64**, 1680–1693, https://doi.org/10.1175/JAS3913.1.

Fyfe, J. C., and O. A. Saenko, 2006: Simulated changes in the extratropical Southern Hemisphere winds and currents. *Geophys. Res. Lett.*, **33**, L06701, https://doi.org/10.1029/2005GL025332.

Grise, K. M., and L. M. Polvani, 2014: Southern Hemisphere cloud–dynamics biases in CMIP5 models and their implications for climate projections. *J. Climate*, **27**, 6074–6092, https://doi.org/10.1175/JCLI-D-14-00113.1.

Hack, J. J., 1994: Parameterization of moist convection in the National Center for Atmospheric Research Community Climate Model (CCM2). *J. Geophys. Res.*, **99**, 5551–5568, https://doi.org/10.1029/93JD03478.

Held, I. M., 2015: Poleward atmospheric energy transport. GFDL, https://www.gfdl.noaa.gov/blog_held/62-poleward-atmospheric-energy-transport.

Hourdin, F., and Coauthors, 2013: LMDZ5B: The atmospheric component of the IPSL climate model with revisited parameterizations for clouds and convection. *Climate Dyn.*, **40**, 2193–2222, https://doi.org/10.1007/s00382-012-1343-y.

Kang, S. M., and L. M. Polvani, 2011: The interannual relationship between the latitude of the eddy-driven jet and the edge of the Hadley cell. *J. Climate*, **24**, 563–568, https://doi.org/10.1175/2010JCLI4077.1.

Kidston, J., and E. P. Gerber, 2010: Intermodel variability of the poleward shift of the austral jet stream in the CMIP3 integrations linked to biases in 20th century climatology. *Geophys. Res. Lett.*, **37**, L09708, https://doi.org/10.1029/2010GL042873.

——, G. K. Vallis, S. M. Dean, and J. A. Renwick, 2011: Can the increase in the eddy length scale under global warming cause the poleward shift of the jet streams? *J. Climate*, **24**, 3764–3780, https://doi.org/10.1175/2010JCLI3738.1.

Le Quéré, C., and Coauthors, 2007: Saturation of the Southern Ocean CO_2 sink due to recent climate change. *Science*, **316**, 1735–1738, https://doi.org/10.1126/science.1136188.

Li, Y., D. W. J. Thompson, and S. Bony, 2015: The influence of atmospheric cloud radiative effects on the large-scale atmospheric circulation. *J. Climate*, **28**, 7263–7278, https://doi.org/10.1175/JCLI-D-14-00825.1.

Lindvall, J., G. Svensson, and R. Caballero, 2017: The impact of changes in parameterizations of surface drag and vertical diffusion on the large-scale circulation in the Community Atmosphere Model (CAM5). *Climate Dyn.*, **48**, 3741–3758, https://doi.org/10.1007/s00382-016-3299-9.

Martin, G. M., and Coauthors, 2011: The HadGEM2 family of Met Office Unified Model climate configurations. *Geosci. Model Dev.*, **4**, 723–757, https://doi.org/10.5194/gmd-4-723-2011.

Menzel, M. E., D. Waugh, and K. Grise, 2019: Disconnect between Hadley cell and subtropical jet variability and response to increased CO_2. *Geophys. Res. Lett.*, **46**, 7045–7053, https://doi.org/10.1029/2019GL083345.

Michel, C., and G. Rivière, 2014: Sensitivity of the position and variability of the eddy-driven jet to different SST profiles in an aquaplanet general circulation model. *J. Atmos. Sci.*, **71**, 349–371, https://doi.org/10.1175/JAS-D-13-074.1.

Neale, R. B., and Coauthors, 2010: Description of the NCAR Community Atmosphere Model (CAM5.0). NCAR Tech. Note NCAR/TN-486+STR, 268 pp., www.cesm.ucar.edu/models/cesm1.1/cam/docs/description/cam5_desc.pdf.

Neggers, R. A. J., J. D. Neelin, and B. Stevens, 2007: Impact mechanisms of shallow cumulus convection on tropical climate dynamics. *J. Climate*, **20**, 2623–2642, https://doi.org/10.1175/JCLI4079.1.

Pithan, F., T. G. Shepherd, G. Zappa, and I. Sandu, 2016: Climate model biases in jet streams, blocking and storm tracks resulting from missing orographic drag. *Geophys. Res. Lett.*, **43**, 7231–7240, https://doi.org/10.1002/2016GL069551.

Shaw, T. A., 2019: Mechanisms of future predicted changes in the zonal mean mid-latitude circulation. *Curr. Climate Change Rep.*, **5**, 345–357, https://doi.org/10.1007/s40641-019-00145-8.

Sherwood, S. C., S. Bony, and J.-L. Dufresne, 2014: Spread in model climate sensitivity traced to atmospheric convective mixing. *Nature*, **505**, 37–42, https://doi.org/10.1038/nature12829.

Simpson, I. R., and L. M. Polvani, 2016: Revisiting the relationship between jet position, forced response, and annular mode variability in the southern midlatitudes. *Geophys. Res. Lett.*, **43**, 2896–2903, https://doi.org/10.1002/2016GL067989.

——, and Coauthors, 2020: An evaluation of the large-scale atmospheric circulation and its variability in CESM2 and other CMIP models. *J. Geophys. Res. Atmos.*, **125**, e2020JD032835, https://doi.org/10.1029/2020JD032835.

——, K. A. McKinnon, F. V. Davenport, M. Tingley, F. Lehner, A. A. Fahad, and D. Chen, 2021: Emergent constraints on the large-scale atmospheric circulation and regional hydroclimate: Do they still work in CMIP6 and how much can they actually constrain the future? *J. Climate*, **34**, 6355–6377, https://doi.org/10.1175/JCLI-D-21-0055.1.

Son, S.-W., and Coauthors, 2010: Impact of stratospheric ozone on Southern Hemisphere circulation change: A multimodel assessment. *J. Geophys. Res.*, **115**, D00M07, https://doi.org/10.1029/2010JD014271.

Staten, P. W., J. Lu, K. M. Grise, S. M. Davis, and T. Birner, 2018: Re-examining tropical expansion. *Nat. Climate Change*, **8**, 768–775, https://doi.org/10.1038/s41558-018-0246-2.

Swart, N. C., and J. C. Fyfe, 2012: Observed and simulated changes in the Southern Hemisphere surface westerly wind-stress. *Geophys. Res. Lett.*, **39**, L16711, https://doi.org/10.1029/2012GL052810.

Taylor, K. E., R. J. Stouffer, and G. A. Meehl, 2012: An overview of CMIP5 and the experiment design. *Bull. Amer. Meteor. Soc.*, **93**, 485–498, https://doi.org/10.1175/BAMS-D-11-00094.1.

Tiedtke, M., 1989: A comprehensive mass flux scheme for cumulus parameterization in large-scale models. *Mon. Wea. Rev.*, **117**, 1779–1800, https://doi.org/10.1175/1520-0493(1989)117<1779:ACMFSF>2.0.CO;2.

Vallis, G. K., P. Zurita-Gotor, C. Cairns, and J. Kidston, 2015: Response of the large-scale structure of the atmosphere to global warming. *Quart. J. Roy. Meteor. Soc.*, **141**, 1479–1501, https://doi.org/10.1002/qj.2456.

Voigt, A., and T. A. Shaw, 2015: Circulation response to warming shaped by radiative changes of clouds and water vapour. *Nat. Geosci.*, **8**, 102–106, https://doi.org/10.1038/ngeo2345.

Wallace, J. M., and P. V. Hobbs, 2006: *Atmospheric Science: An Introductory Survey*. 2nd ed. International Geophysics Series, Vol. 92, Academic Press, 484 pp.

Watt-Meyer, O., and D. M. W. Frierson, 2017: Local and remote impacts of atmospheric cloud radiative effects onto the eddy-driven jet. *Geophys. Res. Lett.*, **44**, 10 036–10 044, https://doi.org/10.1002/2017GL074901.

——, and ——, 2019: ITCZ width controls on Hadley cell extent and eddy-driven jet position and their response to warming. *J. Climate*, **32**, 1151–1166, https://doi.org/10.1175/JCLI-D-18-0434.1.

Waugh, D. W., F. Primeau, T. DeVries, and M. Holzer, 2013: Recent changes in the ventilation of the southern oceans. *Science*, **339**, 568–570, https://doi.org/10.1126/science.1225411.

Webb, M. J., and Coauthors, 2015: The impact of parametrized convection on cloud feedback. *Philos. Trans. Roy. Soc.*, **A373**, 20140414, https://doi.org/10.1098/rsta.2014.0414.

——, and Coauthors, 2017: The Cloud Feedback Model Intercomparison Project (CFMIP) contribution to CMIP6. *Geosci. Model Dev.*, **10**, 359–384, https://doi.org/10.5194/gmd-10-359-2017.

Wilcox, L. J., A. J. Charlton-Perez, and L. J. Gray, 2012: Trends in austral jet position in ensembles of high- and low-top CMIP5 models. *J. Geophys. Res.*, **117**, D13115, https://doi.org/10.1029/2012JD017597.

Wood, T., C. M. McKenna, A. Chrysanthou, and A. C. Maycock, 2020: Role of sea surface temperature patterns for the Southern Hemisphere jet stream response to CO2 forcing. *Environ. Res. Lett.*, **16**, 014020, https://doi.org/10.1088/1748-9326/abce27.

Zhang, G., and N. A. McFarlane, 1995: Sensitivity of climate simulations to the parameterization of cumulus convection in the Canadian Climate Centre general circulation model. *Atmos.–Ocean*, **33**, 407–446, https://doi.org/10.1080/07055900.1995.9649539.